Nano Energy 128 (2024) 109848

Contents lists available at ScienceDirect

Nano Energy

journal homepage: www.elsevier.com/locate/nanoen

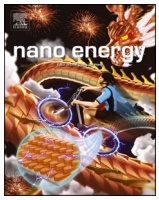

Full paper

Boosting lithium-ion conductivity of polymer electrolyte by selective introduction of covalent organic frameworks for safe lithium metal batteries

Adil Saleem [a], Rashid Iqbal [b], Muhammad Kashif Majeed [c], Arshad Hussain [d], Abdul Rehman Akbar [e], Zawar Hussain [e], Bushra Jabar [f], Sajid Rauf [g], Leon L. Shaw [a,*]

[a] Department of Mechanical, Materials and Aerospace Engineering, Illinois Institute of Technology, Chicago, IL, United States
[b] Key Laboratory of Colloid and Interface Chemistry of the Ministry of Education, School of Chemistry and Chemical Engineering, Shandong University, Jinan 250100, China
[c] Department of Mechanical Engineering, The University of Texas at Dallas, Richardson, TX, United States. Department of Chemistry, School of Natural Sciences, National University of Science and Technology, Islamabad, 44000, Pakistan.
[d] Interdisciplinary Research Center for Hydrogen and Energy Storage, King Fahd University of Petroleum & Minerals, Dhahran 31261, Saudia Arabia
[e] Institute for Advanced Study, Shenzhen University, Shenzhen 518060, China
[f] Institute for Metallic Materials, Leibniz Institute for Solid State and Materials Research Dresden (IFW Dresden), Dresden 01069, Germany
[g] College of Mechatronics and Control Engineering, Shenzhen University, Shenzhen 518060, China

ARTICLE INFO

Keywords:
Lithium metal batteries
Solid electrolyte
Polyethylene oxide
Covalent organic frameworks
Ionic conductivity

ABSTRACT

The demand for high-energy-density batteries has prompted exploration into advanced materials for enhancing the safety and performance of lithium metal batteries (LMBs). This study introduces a novel approach, incorporating two-dimensional (2D) pyrazine and imine-linked covalent organic frameworks (COFs) into a polyethylene oxide (PEO)-based solid electrolyte matrix. The synthesized COFs act as multifunctional additives, improving mechanical strength, ionic conductivity (reaching 1.86 $\times 10^{-3}$ S/cm at room temperature), electrochemical window (oxidation resistance up to 5 V vs. Li/Li^+), and thermal stability (up to 400 °C). The unique electron-rich and polar functionalities of pyrazine and imine linkages facilitate strong interactions with lithium ions (Li^+), resulting in a flexible composite solid electrolyte that mitigates dendrite formation and interface instability. Electrochemical performance of LMBs with $LiNi_{0.8}Mn_{0.1}Co_{0.1}O_2$ (NMC811) cathode further confirm the enhanced Li^+ conductivity, prolonged cycling stability, and a stable solid electrolyte interface, showcasing the potential of COFs in improving LMB performance. Overall, this study highlights the promising role of pyrazine and imine-linked COFs as effective additives for polymer-based solid electrolytes and their potential for developing safer and more efficient LMBs in the future.

1. Introduction

The intrinsically safe solid-state batteries (SSBs) with a potential of higher energy densities than Li-ion batteries (LIBs) have attracted worldwide research endeavors for the last 20 years [1–3]. There is a prevalent belief that solid-state electrolytes (SSEs) can offer a holistic approach to facilitate the integration of the high energy density Li-metal anode with the enhanced safety features of the electrolyte [4,5]. It is anticipated that SSEs with excellent mechanical strength can significantly stop Li-dendrite formation and avoid short circuits while charging/discharging [6]. One of the promising SSEs is polymer-based solid electrolytes (PSEs) which possess manufacturing advantages because of their outstanding film-forming processability, high flexibility for good physical contact with electrodes, leak-free nature, and low processing cost [7–11]. However, their applications in SSBs have been hindered by their low ionic conductivities (typically 10^{-5} to 10^{-8} S/cm) and inferior electrochemical windows [1,7].

The interfacial challenges in SSBs often stem from the volume changes in electrodes during charge/discharge cycles. A significant issue arises as the majority of PSE are incapable of accommodating the volume shift occurring throughout these operations [12]. This incapacity leads to the separation of the PSE from the electrodes, resulting in failure

* Corresponding author.
E-mail address: lshaw2@iit.edu (L.L. Shaw).

https://doi.org/10.1016/j.nanoen.2024.109848
Received 19 March 2024; Received in revised form 3 June 2024; Accepted 4 June 2024
Available online 4 June 2024

[13]. This detachment not only hinders the charge transfer process but also induces the formation of Li dendrites during cycling, as it substantially raises barriers for both electron and ion transportation [14]. Efficiently enhancing and maintaining the compatibility of PSE with electrodes is crucial. One key strategy involves focusing on the development of PSE with high flexibility to optimize compatibility [15]. Since composite solid electrolytes can combine the advantageous feature for all SSEs, they have become a research hotspot in recent years making them an ideal choice for solid state LMBs [16].

Among various PSEs polyethylene oxide (PEO) stands out for its strong Li^+ solvation ability and high dielectric constant [13,17]. However, challenges persist in its low ionic conductivity at ambient temperature, a restricted electrochemical window, and limited electrode compatibility [7,18]. According to the previous reports, nanoparticles demonstrate the capability to form consistent membrane structures for Li^+ transport due to their high interfacial adhesion to the polymer matrix [19]. Covalent organic frameworks (COFs) are an emerging class of organic crystalline porous materials that are created by modular chemistry, where molecular building blocks can be adorned with different redox-active groups that are linked together by covalent bonds [20–23]. These materials are adept at constructing well-defined networks featuring customized channels or functional groups, achieved through the strategic assembly of organic building blocks, commonly utilized in applications related to LIBs [24–26]. In contradistinction to conventional polymer electrolytes, COFs exhibit a substantial inherent free volume resulting from periodic and rigid crystalline structures, thereby conferring an advantageous environment for swift Li^+ conduction. Additionally, their intrinsic porosity facilitates ion conduction by furnishing an abundance of ionic-conducting pathways or accommodating guest species to expedite Li^+ conduction [27]. Moreover, COF materials demonstrate exceptional thermal stability, preserving their structural integrity or undergoing phase transitions at temperatures as elevated as 300 °C [28,29]. This attribute facilitates sustained Li^+ conduction within COFs at elevated temperatures. Owing to these merits, COFs represent an appealing platform for investigating the structure-property relationships of Li^+ conductors [30]. Substantial research efforts have been dedicated to the development of COFs-based electrolytes, driven by the distinctive architectures they offer [31,32]. However, there is still a rising demand for COF-based composite electrolytes with exceptional mechanical strength, exceptional electrochemical window, and superior ionic conductivity.

Herein, we designed two-dimensional (2D) pyrazine-linked covalent organic framework (P-COF) and imine-linked covalent organic framework (I-COF) reinforced PEO-based solid electrolyte with holistically

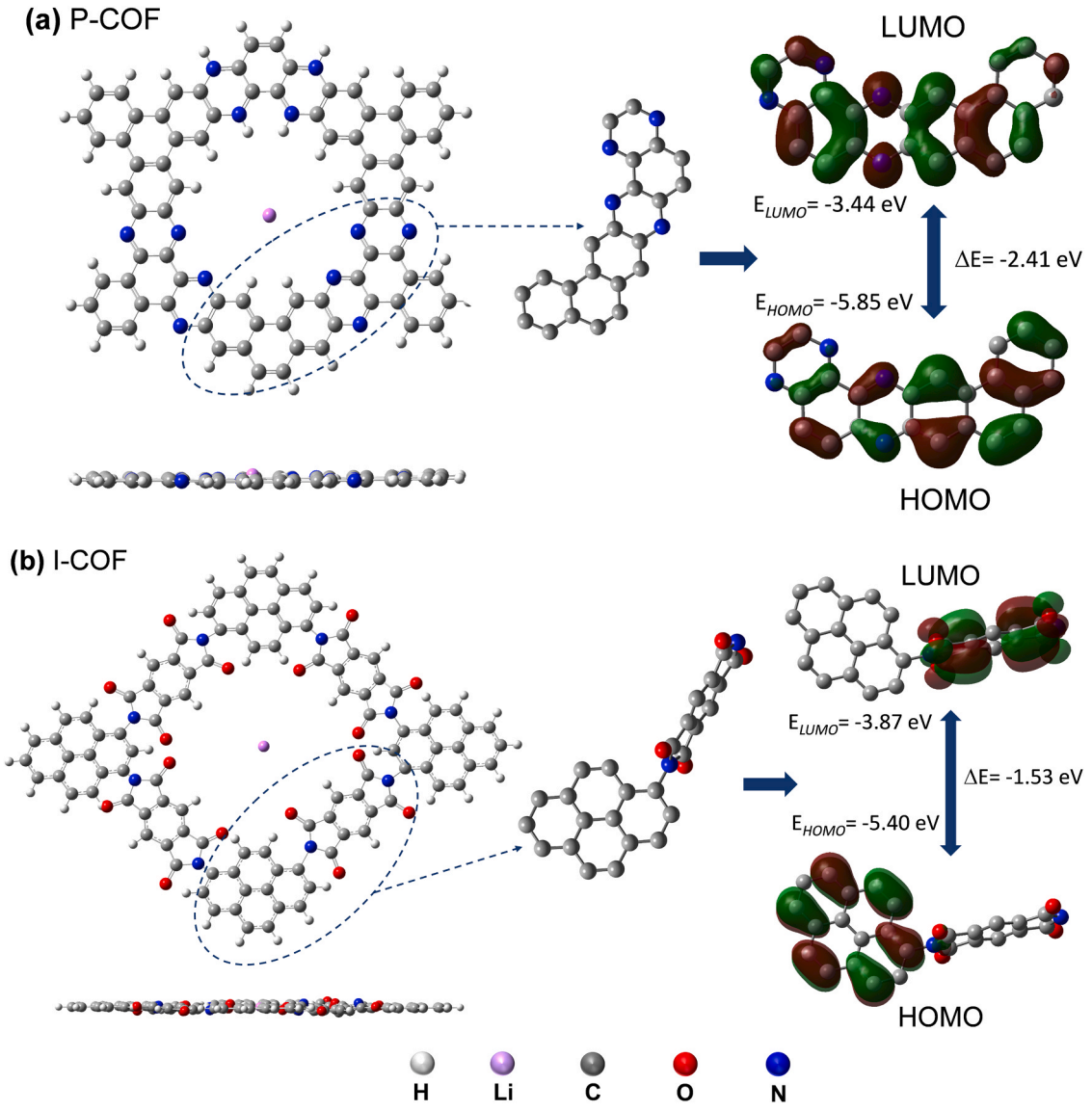

Fig. 1. Optimized structural model of **(a)** P-COF **(b)** I-COF with top view and side view.

oriented ion migration channels for LMBs with enhanced ionic conductivity, thermal and electrochemical stability. To gain more insight into the function of COFs in PEO matrix, the density functional theory (DFT) calculations were caried out as shown in Table S1. Among the well-known COF units comprising characteristic chemical bonds, pyrazine contains two nitrogen atoms in its aromatic ring [33]. The dual redox active sites (C═O and C═N) and the additional N

atoms in P-COF result in enhanced ionic conductivity and Li^+ transport (Fig. 1**a** and **S1a**). The lowest unoccupied molecular orbital (LUMO) energy level of P-COF and I-COF is lower than most organic materials, which implies larger electron affinity and higher reduction potential and thus a high working voltage [34–36]. The smaller highest occupied molecular orbital (HOMO)-LUMO gap also indicates possibly enhanced ionic conductivity [34]. The stable imine-linked conductive network in highly crystalline I-COF with abundant stable and lithium-philic triazine and polyfluorobenerted groups in the skeleton can substantially facilitate the Li^+ transport due to their large conjugated cores and redox reactions of carbonyl groups (Fig. 1**b** and **S1b**). For these reasons I-COF and P-COF have been selected for in-depth investigation in this study. Nonetheless, taking into account the delocalized energy levels, the calculated redox potential of each individual electroactive segment of the COFs might occasionally deviate from the total oxidation-reduction potential of the polymeric band structure. Such a divergence of the redox activity is caused by charge-transfer or electron push-pull processes between the covalently coupled electroactive segments, interactions between the layers, and inter- and intralayer hydrogen bonding in the COFs. COFs are frequently built with a programmed donor-acceptor segment orientation in order to preserve planarity and enable the through-space/through-bond transfer of charge carriers for electronic activity [37]. The ionic interactions are dominated by hopping processes as a result of this charge transfer capacity, which lessens the constraints of electronic conductivity. Charge carrier hopping is further aided by continuous electron flow from centers that are rich in electrons to centers that are poor in electrons, which lowers charge-transfer resistance and improves ionic conductance. These complications further underscore the necessity of investigating I-COF and P-COF reinforced PEO-based SSEs to explore their potentials for enhancing the ionic conductivity and electrochemical stability along with reduced flammability and interface resistance.

2. Results and discussion

An exemplary ionic conductor is expected to manifest minimal resistance to ionic mobility while simultaneously facilitating ion-pair dissociation [38]. Extensive exploration has been conducted on polar groups with the objective of forming associations with Li^+, thereby enhancing ion-pair dissociation within the solid electrolyte. The structured channels inherent in COF materials serve to provide a conducive free volume for the unhindered mobility of Li^+ [39]. Therefore, we first synthesized highly crystalline P-COF and I-COF with the condensation of different monomers through solvothermal method as shown in Figs. 2**a** and 2**b**. The SEM images show a rod like and spherical uniform morphology of P-COF (Fig. 2**c-e**) and I-COF (Fig. 2**f-h**), respectively. The 2D layered structure of COFs were further confirmed with high resolution transmission electron microscopy (HR-TEM). EDS mapping confirms the uniform distribution of carbon, nitrogen, and oxygen elements

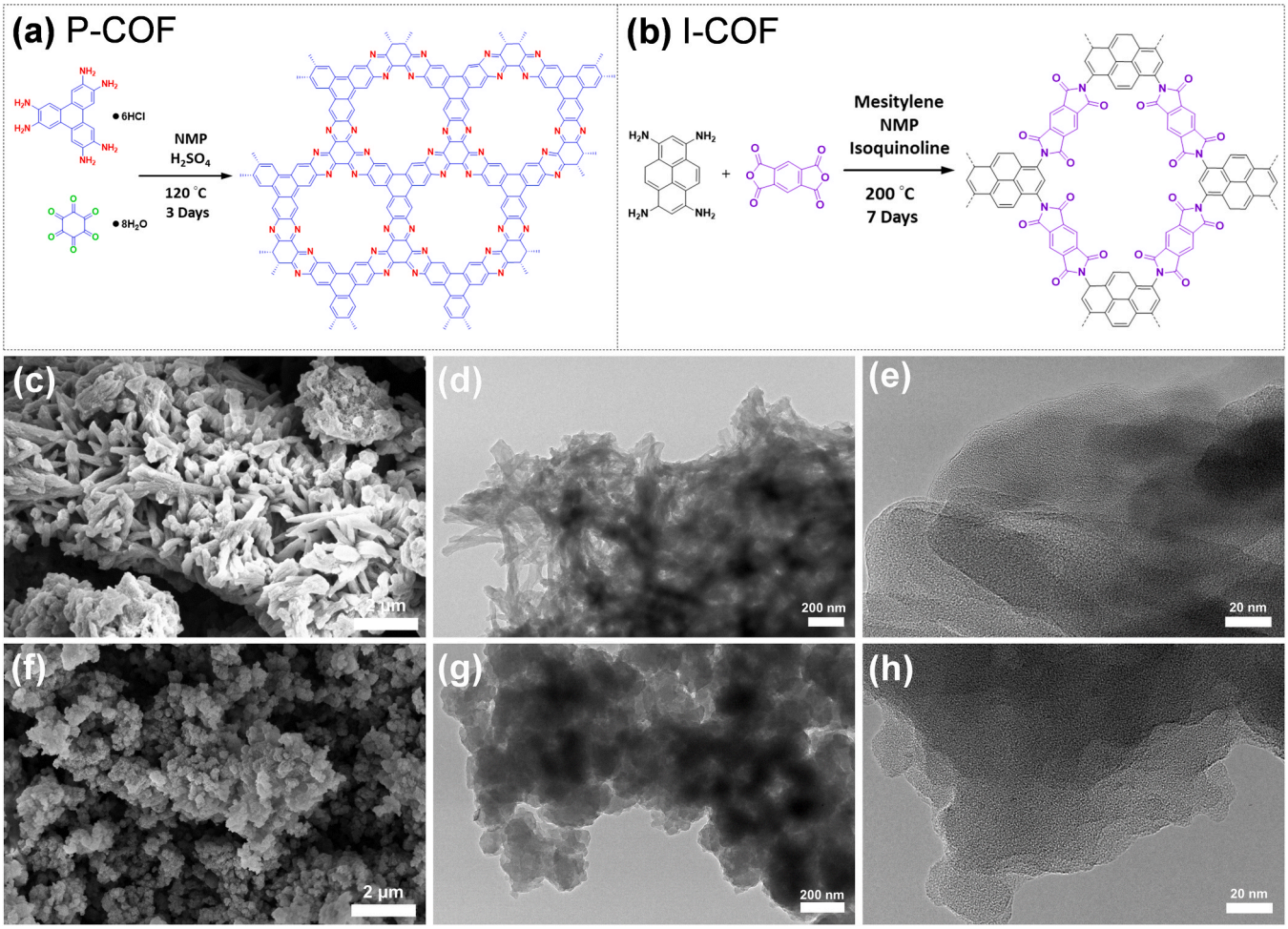

Fig. 2. Schematic illustration of **(a)** P-COF and **(b)** I-COF synthesis process. SEM and HR-TEM images of the magnified **(c-e)** P-COF and **(f-h)** I-COF nanoparticles.

in the as-prepared P-COF and I-COF materials (Figure S2). Powder X-ray diffraction (P-XRD) patterns in Figure S3 reveals a well crystalline structure with strong peaks at 4.7° and 26.2° corresponding to the (100) and (001) diffraction planes, respectively, with some minor peaks at 5.72°, 7.45°, and 9.50° corresponding to the (110), (200), (210), and (220) diffraction planes [40].

The PEO/COF membranes were prepared via a simple and scalable blade casting method. XRD measurements were employed to examine the impact of COF fillers on the crystallization degree of PEO (Figure S4). The semi-crystalline nature of PEO is evident in XRD patterns, with prominent diffraction peaks observed at ~19.2° and ~23.04, and 23.6° [41,42]. Overall, no apparent shift or alteration is observed in the positions of the characteristic diffraction peaks with the introduction of LiTFSI and COF fillers to PEO besides with some additional minor peaks which could be due to the air moisture. However, with the addition of COF fillers there is a minor reduction of the distinctive PEO peaks intensity, implying that the COF fillers may impede the crystallization process of PEO. The SEM images in Fig. 3 show the top (inlet digital

image), bottom and cross-section of the composite electrolyte membranes, which is quite similar to pristine-PEO (P-PEO) electrolyte (Fig. 3**b**). The top surfaces of all the composites exhibit nano pores and the bottom shows a dense structure. The COF network with a porous structure into PEO form a flexible gel-layer, which can improve the Li^+ migration and promote the uniform deposition of Li^+. Overall, due to the different structures and molecular weights of the COF materials the COF-reinforced PEO membranes show a bit different surface morphologies. The cross-section images show the minimum thickness of 29, 33, and 32 μm for P-PEO, PEO/P-COF, and PEO/I-COF, respectively.

As the PEO is mainly composed of semi-crystalline structure which

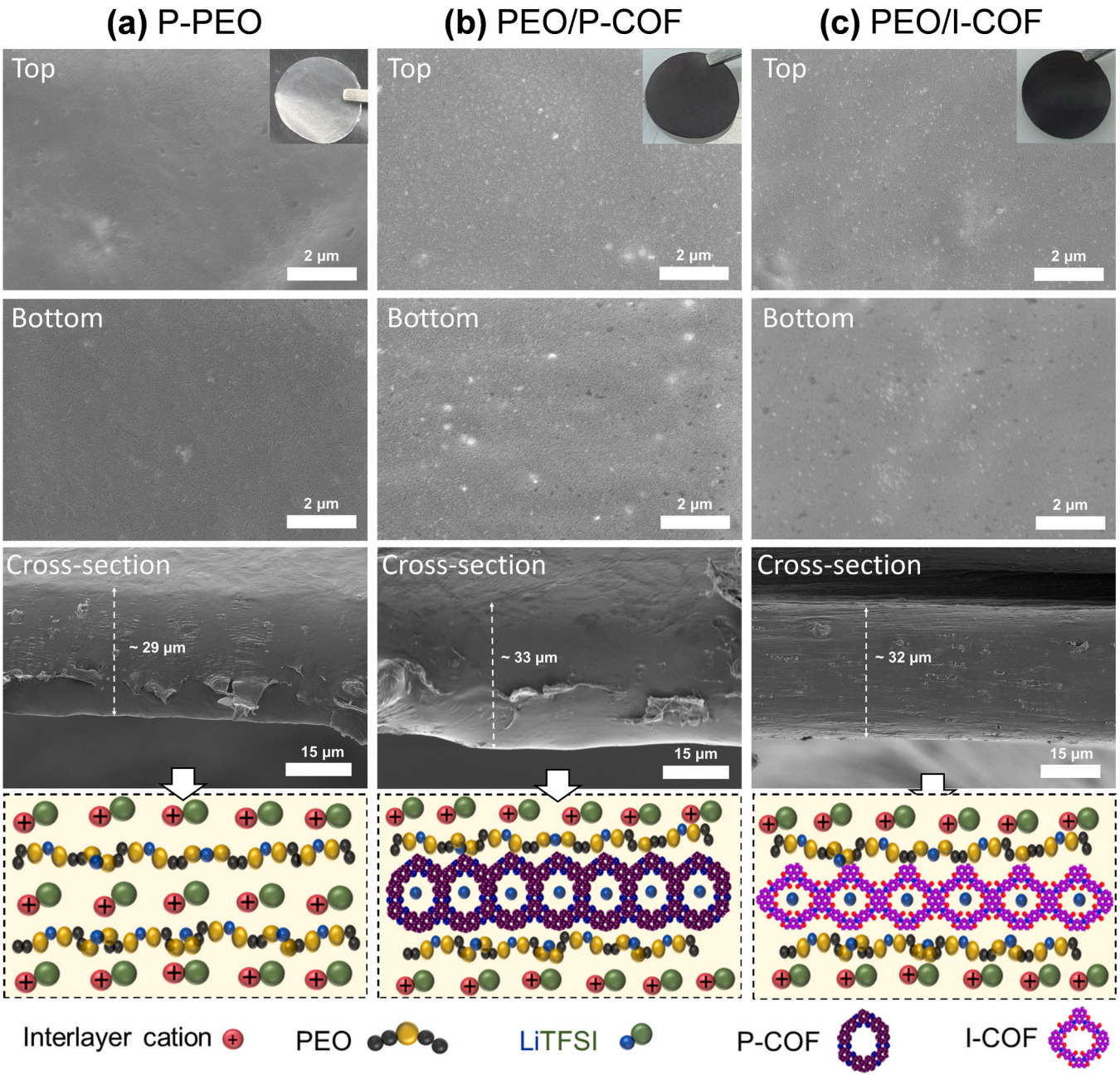

Fig. 3. SEM images of the top (inlet digital image of the membranes), bottom, and cross-section of the (a) P-PEO, (b) PEO/P-COF and (c) PEO/I-COF with schematic presentation of the mechanism for COF fillers in PSE membranes.

can improve the overall ionic conductivity. Additionally, the presence of conductive COF network provides more ion migration path while blocking anion transport leading to reduce the electric field at the cathode electrolyte interface. The redox-active sites in COF fillers appear to have a dual role in promoting segment motion and generating additional free conducting Li^+, potentially enhancing the overall performance of the battery. In the schematic (Fig. 3), the structural illustration of P-PEO, PEO/P-COF, and PEO/I-COF shows the surface electronegative channels in COF fillers, facilitating the LiTFSI dissociation in PEO/COF membranes along with its own surface absorbed Li^+ and thus generating more conducting Li^+ ions. In addition, the energy dispersive spectroscopy (EDS) mapping confirms the uniform distribution of COF fillers in composite electrolyte membranes (Figure S5).

Fig. 4**a** displays the Fourier-transform infrared (FT-IR) spectra attributing to the chemical and structural changes in P-PEO and composite electrolytes. The absorption peaks observed at ~1467, 1098, and 841 cm^{-1} can be attributed to the -CH_2 scissoring mode, C-O-C stretching mode, and -CH_2 wagging mode, respectively. Notably, no novel distinctive features are discerned, except for the typical inherent peaks associated with PEO and LiTFSI. This observation suggests that the incorporation of COFs additives exerts no discernible impact on the microscopic structure, potentially attributed to their minimal concentration within the system. The primary concern for battery safety is thermal runaway, triggered by internal short circuits resulting from thermal shrinkage of the separator and the penetration of Li-dendrites. It is crucial for the separator to retain its mechanical integrity at elevated temperatures to prevent physical contact between electrodes and the potential risk of internal short circuits. The TGA curves in Fig. 4**b** illustrate that the introduction of COF materials significantly enhances the thermal decomposition temperature of PEO matrix from ~250 °C (P-PEO) to ~400 °C (PEO/P-COF and PEO/I-COF) [43]. Such a high decomposition temperature meets completely the requirement of PSE for industrial application. The breakdown curve of P-PEO observed in the thermogravimetric analysis (TGA) aligns with the trend of thermogravimetric loss due to the absence of COF nanoparticles in the membrane. In the flammability test, rectangles cut from the PSE

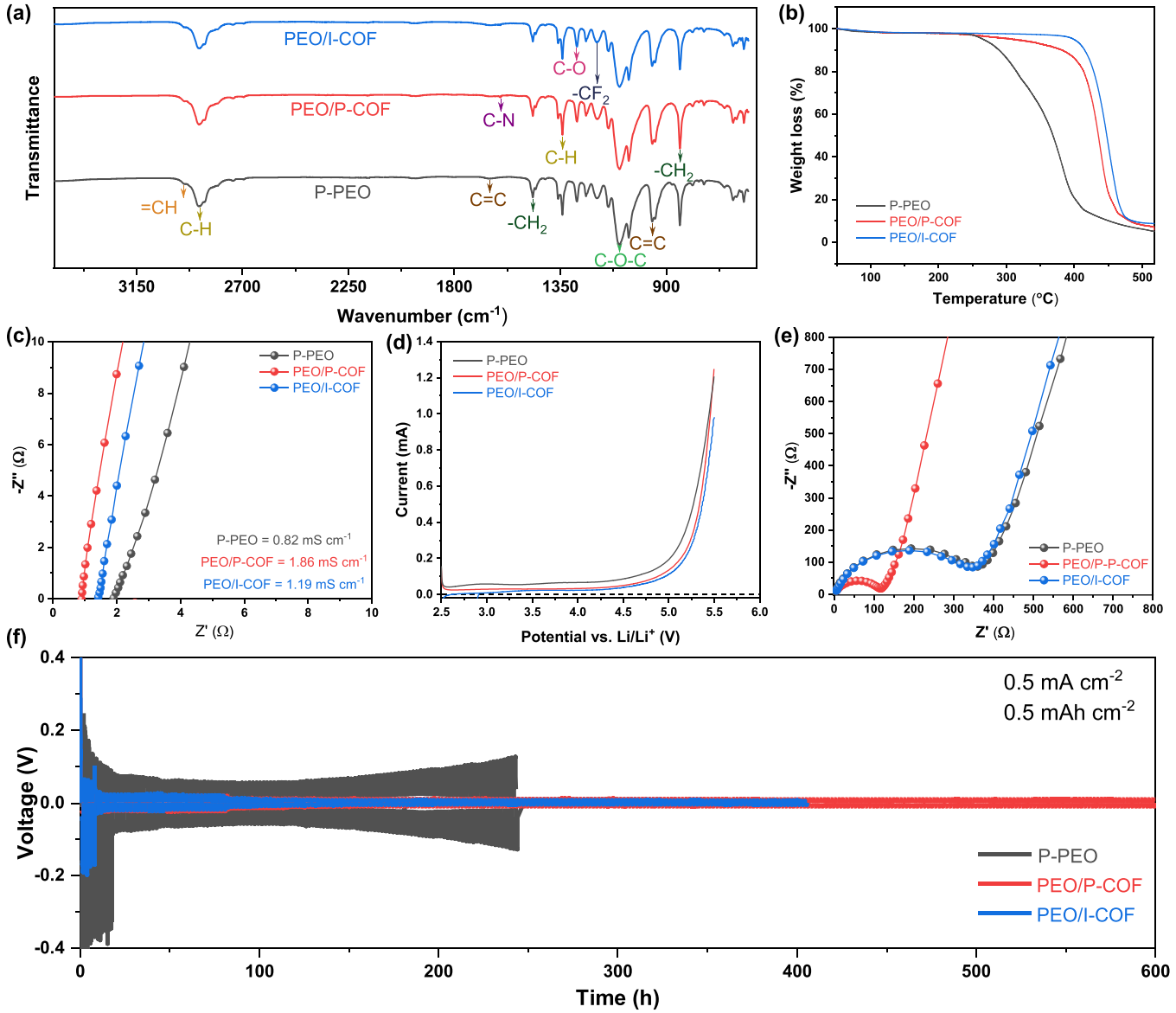

Fig. 4. **(a)** FT-IR spectra and **(b)** TGA curves of P-PEO, PEO/P-COF and PEO/I-COF membranes. **(c)** Electrochemical impedance spectra (EIS) with ionic conductivity values for P-PEO, PEO/P-COF and PEO/I-COF membranes. **(d)** LSV of SS/PSE/Li cells at 0.5 mV s^{-1} scan rate. **(e)** Nyquist plots for the Li/PSE/Li symmetric cells before cycles. **(f)** Voltage profile of Li-plating/striping cycles of Li/PSE/Li batteries with the current density and plating/striping capacity indicated in the figure.

membranes were exposed to an alcohol flame (Figure S6a). As the P-PEO membrane approached the flame, it exhibited coiling and completely melted to transparent state in a short time, whereas the PEO/P-COF and PEO/I-COF membranes only displayed color change upon contact with the flame, indicating carbonization and flame-retardant properties [44]. Additionally, the PEO/P-COF membrane exhibited curling in proximity to the flame. These findings affirm that the PEO/COF membranes, particularly PEO/I-COF, possess high degrees of flame retardancy and thermal stability, thereby reducing the likelihood of thermal runaway and ensuring battery safety.

Figures S6b and S7 display the digital images of stretching and folding tests for all the electrolytes. As shown in Figure S6b, P-PEO membrane cracks when being stretched to 43 mm, whereas PEO/P-COF membrane exhibits no cracks when being stretched to 50 mm. PEO/I-COF membrane also has good mechanical stability, showing no cracks when stretching to 43 mm. The folding experiments shown in Figure S7 demonstrate that the composite membranes can fully recover even after 360° folding. These digital images of stretching and folding tests show the excellent flexibility of PEO/P-COF and PEO/I-COF composite membranes. Overall, the introduction of COF networks in PEO provides a stable dimensional structure with excellent flexibility which expands the operating conditions of solid-state LMBs.

To explore the effect of COFs on the ionic conductivity of PSE membranes, PSE membranes were sandwiched between two stainless steels (SSs) in coin cell (2032) at room temperature. This method is commonly employed to mitigate interfacial impedance without introducing alterations to the solid structure of the membrane, distinguishing it from gel electrolytes. It can be seen in Fig. 4**c**, PSE membranes containing COFs deliver higher ionic conductivity as compared to the P-PEO (0.82 mS/cm^2) and many of the reported work (Table S2). In addition, PEO/P-COF membrane shows a maximum ionic conductivity of 1.86 $\times 10^{-3}$ S/cm^2, higher than that of PEO/I-COF membrane (1.19 $\times 10^{-3}$ S/cm^2) corresponding to the construction of fast ion transport channel, which might be due to the higher redox active groups providing efficient pathways for Li^+ conduction in P-COF. The high ionic conductivities achieved here can be attributed to three (3) mechanisms. The first is the addition of Li-salt (such as LiTFSI in this study) into PEO, which grafts the anion to the PEO polymer chain and allows the Li^+ cation to (relatively) move more freely. However, too high salt contents could restrict the mobility of the individual charge carriers and reduce the mechanical properties. Therefore, we have used the PEO:LiTFSI molar ratio in 10:1 in this study (which is comparatively low). The second mechanism is achieved by adding plasticizers, which can decrease the crystallinity of polymers and thus increase the mobility of Li ions in the electrolytes [45]. In this work we have used a minute amount of tetraethylene glycol dimethyl ether (TEGDME) plasticizer, which helps improve the overall ionic conductivity for all the samples (particularly P-PEO membrane). The last mechanism for the high ionic conductivity achieved in this work is through the addition of COFs. The COF's crosslinking sites develop a network skeleton structure in PEO, offering ion migration channels while inhibiting the anion movement and thus leading to further improvement in ionic conductivity over P-PEO.

Linear sweep voltammetry (LSV) was conducted to evaluate the electrochemical operational window of PSE membranes on the SSs/PSE/Li-metal in a coin cell. The maximum value of electrochemical decompose potential for P-PEO, PEO/P-COF, and PEO/I-COF are found to be 4.6, 4.8, and 5.0 V, respectively (Fig. 4**d**). The best oxidation resistance of PEO/I-COF membrane is attributed to the introduction of I-COF as crosslinking sites which can significantly stabilize the polymer chains and prevent the decomposition of PEO matrix. The Nyquist plots for Li/PSE/Li symmetric cells are presented in Fig. 4**e**. Typically, the EIS impedance of cells comprises electrolyte resistance (R_e), SEI resistance (R_f), and charge transfer resistance (R_{ct}), respectively. The Li^+ with P-COF polymer electrolytes exhibits efficient and rapid charge transfer as compared to P-PEO and PEO/I-COF composite. This is evident from the shortened intercept and reduced radius observed in the electrochemical impedance spectroscopy data, indicating a notable decrease in resistance. The favorable changes in these parameters suggest improved performance and reliability of the battery, particularly in terms of enhanced charge transfer characteristics.

In order to assess the cation selectivity, lithium transfer number (t_{Li}^+) values were measured, which signifies the percentage of Li^+ in the total current. This measurement was conducted through conventional Bruce-Vincent technique [46]. In Figure S8, P-COF showed a maximum value of t_{Li}^+, which were calculated by analyzing the DC-polarization and EIS spectra. The COF's crosslinking sites develop a network skeleton structure in PSE which can inhibit the anion movement, hence improving the overall t_{Li}^+. Meanwhile, P-COF have abundant active site (C═O and C═N) and the additional N atoms which can provide more conduction pathways to maximize the Li^+ transfer efficiency. As such, the measured t_{Li}^+ value for PEO/P-COF (0.28) is higher than those of P-PEO (0.12) and PEO/I-COF (0.13). A higher t_{Li}^+ number enable a high Li^+ flux in LMBs. Overall, the COF containing membranes demonstrate its function with a cationic highway for speeding Li^+ transport by exhibiting a high Li^+ transference number and strong ionic conductivity at room temperature under ideal electronegativity conditions.

The galvanostatic cycling performance of symmetric cells (Li-metal/PSE/Li-metal) were tested at current density of 0.5 mA/cm^2 at room temperature. As shown in Fig. 4**f and S9** (enlarged view), the coin cell with PEO/P-COF and PEO/I-COF membrane displayed a more stable cycling performance for at least 600 and 400 h, respectively, with a stable voltage profile. The symmetric cell with P-PEO shows significantly larger polarization as compared to PEO/P-COF and PEO/I-COF. However, PEO/P-COF exhibits an excellent stable and flat voltage plateau for 600 h period showing good interface compatibility. The poor cyclability observed in P-PEO is attributed to the uneven and irregular flow of Li^+ on the surfaces of Li metals, leading to the dendrite formation. Conversely, membranes containing COFs exhibited significantly improved overpotential and enhanced cyclability during Li plating and stripping processes. This improvement stems from the well-defined 2D channels provided by COF fillers, which facilitates a consistent flow of Li^+ towards the Li metal electrode. Moreover, P-COF membranes may guide Li^+ migration within these channels, thereby accelerating Li^+ movement, particularly due to the presence of rich redox-active regions.

In order to analyze the industrial applications of the as-prepared PSE membranes, a 2032-type coin cell were assembled with commercially available $LiNi_{0.8}Mn_{0.1}Co_{0.1}O_2$ (NMC811) cathode. Full cells with NMC811/PSE/Li-metal were assembled to study the cycling and rate performance. Fig. 5**a** presents the rate performance of full cells for PSEs at different current rates (0.2 C, 0.5 C, 1 C, 2 C, and 3 C; where 1 C = 200 mA/g), showing a maximum capacity of 146.4 mAh/g at 0.2 C for PEO/P-COF composite electrolyte. These results demonstrate the great potential of PEO/COF composite electrolytes for the application of high energy density LMBs. Fig. 5**b** shows the cycle performance for PSE electrolytes at 0.5 C for 100 cycles. The PEO/P-COF composite exhibits a maximum specific capacity of 145 mAh/g, whereas PEO/I-COF and P-PEO provide lower maximum specific capacities of 142 mAh/g and 141

mAh/g, respectively. The coin-cell with I-COF delivers a reversible capacity of 134 mAh/g after 100 cycles with a high coulombic efficiency of 99 %. In contrast, the P-PEO coin cell shows a visible declined reversible capacity (106 mAh/g) after 100 cycles.

Fig. 5**c-e** presents the charge/discharge voltage plot after 5th, 50th, and 100th cycles, exhibiting nearly constant voltage lag corresponding to the improved electrochemical reaction kinetics. To investigate the kinetics of PSE membranes, the impedance of coin cells was measured before and after cycling via EIS. The results before cycling (Figure S10a), reveals that the interfacial impedances of the cells are solely composed of R_e and R_{ct}, suggesting the absence of a protective layer on the electrodes. In contrast, after cycling (Figure S10b) the interfacial impedances include R_e, R_f, and R_{ct}, indicating the presence of protective layers on the electrode surfaces

NMC811/PSE/Li-metal cells were also evaluated for their long-term

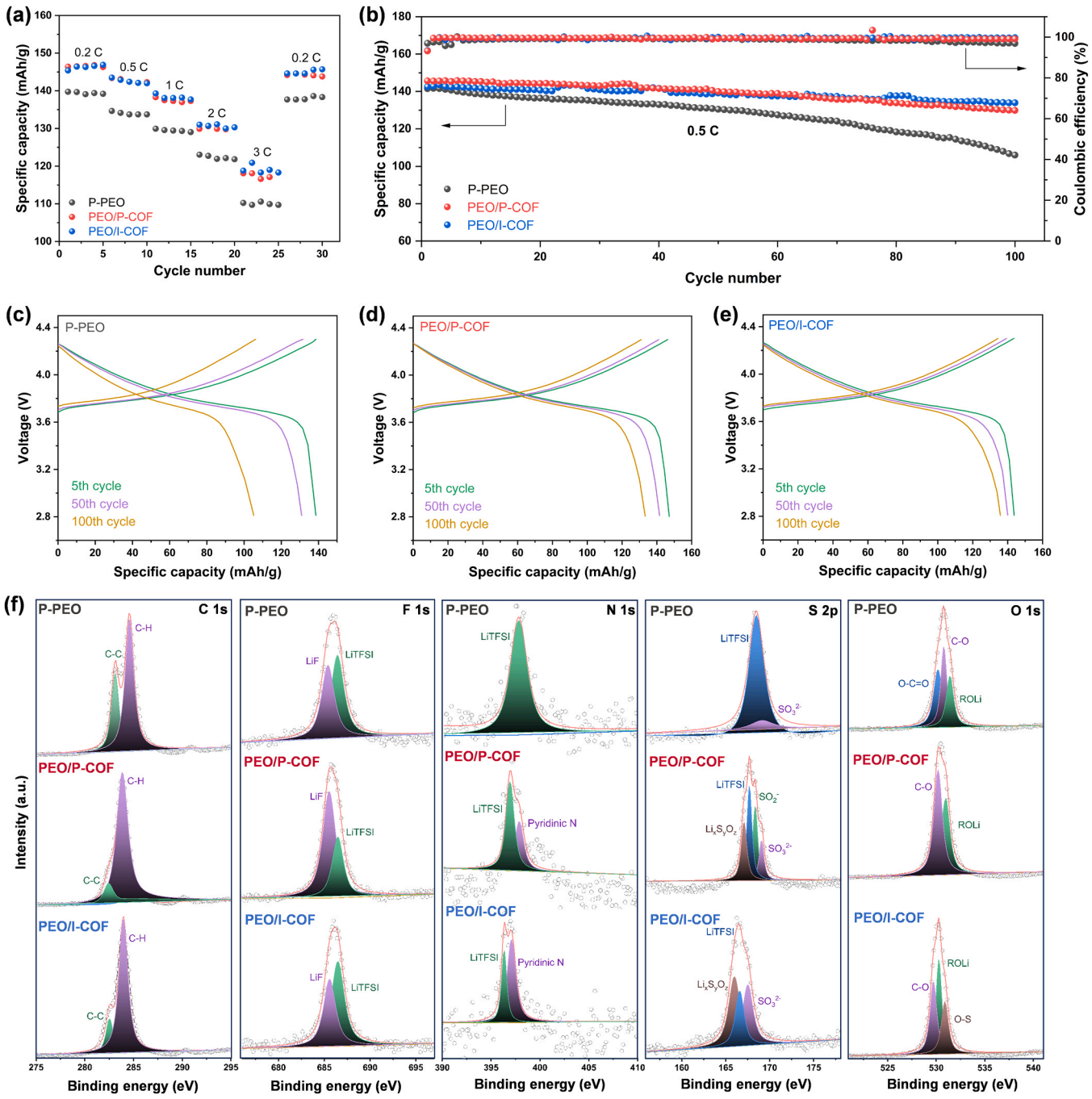

Fig. 5. Electrochemical performances of NMC811/PSE/Li-metal. **(a)** Rate performance, and **(b)** cycle performance of NMC811/PSE/Li-metal. **(c-e)** Charge/discharge curves of NMC811/PSE/Li-metal. **(f)** XPS spectra of C 1 s, F 1 s, N1s, S 2p, and O 1 s of the cycled PSE membranes.

cycle stabilities. As shown in Figure S11, both PEO/P-COF and PEO/I-COF cells offer much better cycle stability than P-PEO cell. Specifically, PEO/P-COF and PEO/I-COF cells exhibit 78 and 86 % capacity retention after 350 cycles. In contrast, P-PEO cell has lost ~41 % of its specific capacity even after only 130 cycles. The poor cycle stability of P-PEO cell is attributed to the poor compatibility of pure solid-state PEO-based electrolyte with NMC and Li metal, leading to irreversible side reactions in a working battery to cause great capacity loss. However, addition of the COF material helps retard the capacity attenuation of NMC/PSE/Li batteries, owing to the aforementioned improvement in the resistance against electrochemical oxidation (Fig. 4**d**), good interface compatibility with Li metal (Fig. 4**f**), and fast Li^+ flux enabled by the COF fillers (Fig. 4**c**). It is interesting to note that PEO/P-COF cell has a higher specific capacity than PEO/I-COF cell initially because PEO/P-COF has higher ionic conductivity than PEO/I-COF (Fig. 4**c**) owing to the dual redox active sites (C═O and C═N) and the additional N atoms in P-COF. However, PEO/I-COF cell exhibits better cycle stability than PEO/P-COF cell (Fig. 5**b and S11**), likely due to the higher oxidation resistance of PEO/I-COF than PEO/P-COF (Fig. 4**d**) and better compatibility with Li anode (to be discussed below). Overall, the cycle performance of PEO/COF cells in this work outperform those of previously reported PEO and COF-based ionic electrolytes (Table S3), underscoring the importance of the rational design of the COFs which are featured with electronegativity-rich 2D channels.

The compatibility of PSE membranes with NMC811 cathode were investigated with X-ray photoelectron spectroscopy (XPS) after cycling

(Fig. 5f). The C and O peaks in C 1 s and O 1 s are mainly attributed to the PEO and the strong peaks in F 1 s and S 2p are mainly correspond to the LiTFSI. Additionally, a strong N peaks in N 1 s for P-PEO membrane appears due the LiTFSI, however, for the pyridinic/pyrrolic-N peak correspond to the redox active group of P-COF and I-COF materials. Additionally, an interfacial phase composed of the organic and inorganic phase was also observed. According to available reports, this multicomponent interfacial phase plays a significant role in preserving the compatibility between the electrode and electrolyte [13]. Notably, LiF emerges as a pivotal component within this interfacial phase, characterized by a high ionic conductivity [47]. This heightened ionic conductivity contributes significantly to stabilizing the compatibility between the electrode and electrolyte, underlining the importance of LiF in enhancing overall stability in the system [48]. Overall, no obvious

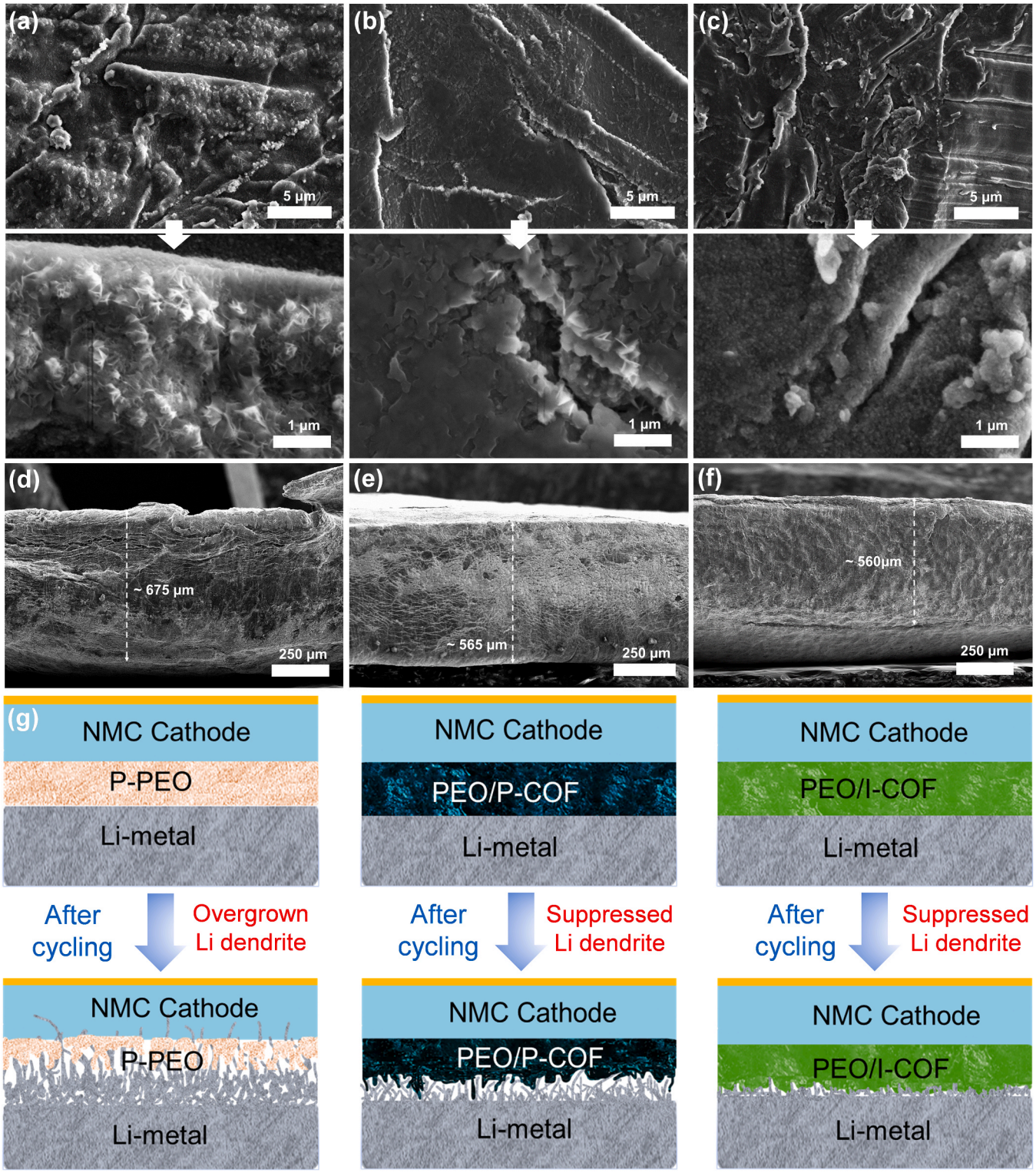

Fig. 6. SEM images of the Li-metal **(a-c)** surface and **(d-f)** cross-section after cycling for P-PEO, PEO/P-COF and PEO/I-COF membranes. **(g-i)** Schematic illustration of the Li-metal dendrite growth during cycling for P-PEO, PEO/P-COF and PEO/I-COF membranes.

signal was detected on PSE membranes in XPS results attributing to a good compatibility with cathode.

The impedance of PEO-based polymer electrodes in the presence of an electric field applied to the Li anode tends to rise. This phenomenon is associated with the destruction of the anode's morphology and the subsequent uneven deposition of Li^+ ions on the surface, leading to the formation of dendrites (Fig. 6**a-c**). In contrast, the PEO/P-COF electrolyte facilitates rapid diffusion of Li^+ ions. This fast diffusion encourages a more uniform deposition of Li^+ ions on the surface of the Li anode, mitigating the formation of dendrites and promoting a more homogeneous distribution. Overall, the COFs containing PEO electrolyte showed a smooth surface as compared to P-PEO membrane, which showed a lumpy and dendrite growth on Li-metal electrode. The addition of COFs with crosslinking network improvs the overall mechanical strength of PEO membrane leading to the longer cycle life. The synergistic effect of mechanical strength, higher ionic conductivity, and higher Li^+ conduction collectively improve the cycle performance and inhibit the growth of Li-dendrite. The presence of Li-dendrites induces finger-like pore structures, potentially causing internal short circuits in batteries and leading to rapid battery failure (Figs. 6**d and** 6**g**). In contrast, the PEO containing P-COF nanoparticles exhibit a sponge-like pore structure (Figs. 6**e and** 6**h**), whereas PEO/I-COF displays a gradual reduction in pore size, resulting in a more uniform cross-

section (Figs. 6**f and** 6**i**). These structural features contribute to enhanced permeability and impede the formation of Li-dendrites. The observed outcomes are

attributed to the establishment of homogeneous Li^+ flow channels within the PSE electrolyte, arising from the high interfacial adhesion between nanoscale particles and the polymer matrix. The COFs-containing membranes act as an effective ion sieve, as depicted in schematic diagram (Fig. 6**g-i**), allowing swift and uniform travel of Li^+, which are evenly deposited on the negative electrode. In contrast, the P-PEO shows a random scattering and non-uniform deposition of Li^+ on the negative electrode following their passage. In general, the conceptualization of a PEO/COFs electrolyte delineates the practical applications of establishing uninterrupted ion transport pathways within PSEs through the incorporation of a 2D COFs network. The inventive framework proposed in this study presents a viable strategy for the tangible realization of solid-state LMBs in practical applications.

3. Conclusions

In summary, the integration of pyrazine and imine-linked COFs into a PEO-based solid electrolyte represents a significant advancement in the pursuit of safer and more efficient LMBs. Through systematic exploration, we have demonstrated that the incorporation of these COFs contributes multifunctional benefits to the solid electrolyte matrix, addressing critical challenges associated with Li-dendrite formation, electrode-electrolyte instability, and thermal safety concerns. The unique combination of electron-rich and polar functionalities within the COFs facilitates strong interactions with Li^+, leading to improved ion conductivity and stability. Electrochemical characterization has provided compelling evidence for the positive impact of COFs on the performance of LMBs. The promising results presented here highlight the potential of pyrazine and imine-linked COFs as effective additives for solid electrolytes, offering a viable strategy for overcoming existing limitations in LMBs.

CRediT authorship contribution statement

Adil Saleem: Writing – original draft, Software, Methodology, Investigation, Formal analysis, Data curation, Conceptualization. Rashid Iqbal: Writing – review & editing, Investigation, Formal analysis, Conceptualization. **Muhammad K. Majeed:** Writing – review & editing, Formal analysis, Conceptualization. **Arshad Hussain:** Methodology, Formal analysis, Data curation. **Abdul Rehman Akbar:** Methodology, Investigation, Formal analysis, Data curation. **Zawar Hussain:** Methodology, Investigation, Formal analysis, Data curation. **Bushra Jabar:** Methodology, Investigation, Formal analysis, Data curation. **Sajid Rauf:** Formal analysis, Data curation. **Leon L Shaw:** Writing – review & editing, Supervision, Project administration, Investigation, Funding acquisition, Formal analysis.

Declaration of Competing Interest

The authors declare that they have no known competing financial interests or personal relationships that could have appeared to influence the work reported in this paper.

Data Availability

Data will be made available on request.

Acknowledgements

This research was financially supported by the U.S. National Science Foundation (NSF) with the award numbers OISE-2230770. LS is also grateful to the Rowe Family Endowment Fund.

Supporting Information

Supplementary data to this article can be found online.

Appendix A. Supporting information

Supplementary data associated with this article can be found in the online version at doi:10.1016/j.nanoen.2024.109848.

References

[1] A. Manthiram, X. Yu, S. Wang, Lithium battery chemistries enabled by solid-state electrolytes, Nat. Rev. Mater. 2 (4) (2017) 16103.
[2] J. Schnell, T. Günther, T. Knoche, C. Vieider, L. Köhler, A. Just, M. Keller, S. Passerini, G. Reinhart, All-solid-state lithium-ion and lithium metal batteries – paving the way to large-scale production, J. Power Sources 382 (2018) 160–175.
[3] J. Ma, B. Chen, L. Wang, G. Cui, Progress and prospect on failure mechanisms of solid-state lithium batteries, J. Power Sources 392 (2018) 94–115.
[4] M. Dirican, C. Yan, P. Zhu, X. Zhang, Composite solid electrolytes for all-solid-state lithium batteries, Mater. Sci. Eng.: R: Rep. 136 (2019) 27–46.
[5] Y. Meesala, A. Jena, H. Chang, R.-S. Liu, Recent advancements in Li-ion conductors for all-solid-state Li-ion batteries, ACS Energy Lett. 2 (12) (2017) 2734–2751.
[6] J. Wu, L. Yuan, W. Zhang, Z. Li, X. Xie, Y. Huang, Reducing the thickness of solid-state electrolyte membranes for high-energy lithium batteries, Energy Environ. Sci. 14 (1) (2021) 12–36.
[7] Z. Ding, J. Li, J. Li, C. An, Review—interfaces: key issue to be solved for all solid-state lithium battery technologies, J. Electrochem. Soc. 167 (7) (2020) 070541.
[8] Y. Shan, L. Li, X. Chen, S. Fan, H. Yang, Y. Jiang, Gentle haulers of lithium-ion–nanomolybdenum carbide fillers in solid polymer electrolyte, ACS Energy Lett. 7 (7) (2022) 2289–2296.
[9] X. He, Y. Ni, Y. Hou, Y. Lu, S. Jin, H. Li, Z. Yan, K. Zhang, J. Chen, Insights into the ionic conduction mechanism of quasi-solid polymer electrolytes through multispectral characterization, Angew. Chem. 133 (42) (2021) 22854–22859.
[10] X. Pei, Y. Li, T. Ou, X. Liang, Y. Yang, E. Jia, Y. Tan, S. Guo, N. Li, Interaction induced deep eutectic gel polymer electrolyte for high performance lithium-metal batteries, Angew. Chem. 134 (31) (2022) e202205075.
[11] J. Zheng, B. Perry, Y. Wu, Antiperovskite superionic conductors: a critical review, ACS Mater. Au 1 (2) (2021) 92–106.
[12] R. Fang, H. Xu, B. Xu, X. Li, Y. Li, J.B. Goodenough, Reaction mechanism optimization of solid-state Li–S batteries with a PEO-based electrolyte, Adv. Funct. Mater. 31 (2) (2021) 2001812.
[13] T. Deng, L. Cao, X. He, A.-M. Li, D. Li, J. Xu, S. Liu, P. Bai, T. Jin, L. Ma, M. A. Schroeder, X. Fan, C. Wang, In situ formation of polymer-inorganic solid-electrolyte interphase for stable polymeric solid-state lithium-metal batteries, Chem 7 (11) (2021) 3052–3068.
[14] C. Wang, K.R. Adair, J. Liang, X. Li, Y. Sun, X. Li, J. Wang, Q. Sun, F. Zhao, X. Lin, Solid-state plastic crystal electrolytes: effective protection interlayers for sulfide-based all-solid-state lithium metal batteries, Adv. Funct. Mater. 29 (26) (2019) 1900392.
[15] X. Zeng, L. Dong, J. Fu, L. Chen, J. Zhou, P. Zong, G. Liu, L. Shi, Enhanced interfacial stability with a novel boron-centered crosslinked hybrid polymer gel electrolytes for lithium metal batteries, Chem. Eng. J. 428 (2022) 131100.

[16] D. Xu, J. Su, J. Jin, C. Sun, Y. Ruan, C. Chen, Z. Wen, In situ generated fireproof gel polymer electrolyte with Li6. 4Ga0. 2La3Zr2O12 as initiator and ion-conductive filler, Adv. Energy Mater. 9 (25) (2019) 1900611.
[17] Q. Kang, Z. Zhuang, Y. Liu, Z. Liu, Y. Li, B. Sun, F. Pei, H. Zhu, H. Li, P. Li, Y. Lin, K. Shi, Y. Zhu, J. Chen, C. Shi, Y. Zhao, P. Jiang, Y. Xia, D. Wang, X. Huang, Engineering the structural uniformity of gel polymer electrolytes via pattern-guided alignment for durable, safe solid-state lithium metal batteries, Adv. Mater. 35 (38) (2023) 2303460.
[18] L. Su, X. Zhao, M. Yi, H. Charalambous, H. Celio, Y. Liu, A. Manthiram, Uncovering the solvation structure of LiPF6-based localized saturated electrolytes and their effect on LiNiO2-based lithium-metal batteries, Adv. Energy Mater. 12 (36) (2022) 2201911.
[19] C. Klaysom, S.-H. Moon, B.P. Ladewig, G.Q.M. Lu, L. Wang, The influence of inorganic filler particle size on composite ion-exchange membranes for desalination, J. Phys. Chem. C. 115 (31) (2011) 15124–15132.
[20] Y. Min, L. Guo, G. Wei, D. Xian, B. Zhang, L. Wang, Enhancing the safety and cyclic performance of lithium-ion batteries using heat resistant and wettable separator based on covalent organic framework and polybenzimidazole, Chem. Eng. J. 443 (2022) 136480.
[21] Y. Xu, Y. Zhou, T. Li, S. Jiang, X. Qian, Q. Yue, Y. Kang, Multifunctional covalent organic frameworks for high capacity and dendrite-free lithium metal batteries, Energy Storage Mater. 25 (2020) 334–341.
[22] C.S. Diercks, O.M. Yaghi, The atom, the molecule, and the covalent organic framework, Science 355 (6328) (2017) eaal1585.
[23] S. Haldar, A. Schneemann, S. Kaskel, Covalent organic frameworks as model materials for fundamental and mechanistic understanding of organic battery design principles, J. Am. Chem. Soc. 145 (25) (2023) 13494–13513.
[24] Z. Liu, K. Zhang, G. Huang, S. Bian, Y. Huang, X. Jiang, Y. Pan, Y. Wang, X. Xia, B. Xu, Lithium-ion transport in covalent organic framework membrane, Chem. Eng. J. 433 (2022) 133550.
[25] K. Geng, T. He, R. Liu, S. Dalapati, K.T. Tan, Z. Li, S. Tao, Y. Gong, Q. Jiang, D. Jiang, Covalent organic frameworks: design, synthesis, and functions, Chem. Rev. 120 (16) (2020) 8814–8933.
[26] D. Jiang, Covalent organic frameworks: an amazing chemistry platform for designing polymers, Chem 6 (10) (2020) 2461–2483.
[27] D. Zhu, G. Xu, M. Barnes, Y. Li, C.-P. Tseng, Z. Zhang, J.-J. Zhang, Y. Zhu, S. Khalil, M.M. Rahman, R. Verduzco, P.M. Ajayan, Covalent organic frameworks for batteries, Adv. Funct. Mater. 31 (32) (2021) 2100505.
[28] Y. Lu, Y. Cai, Q. Zhang, J. Chen, Structure–performance relationships of covalent organic framework electrode materials in metal-ion batteries, J. Phys. Chem. Lett. 12 (33) (2021) 8061–8071.
[29] Z. Wang, W. Jin, X. Huang, G. Lu, Y. Li, Covalent organic frameworks as electrode materials for metal ion batteries: a current review, Chem. Rec. 20 (10) (2020) 1198–1219.
[30] X.-T. Li, J. Zou, T.-H. Wang, H.-C. Ma, G.-J. Chen, Y.-B. Dong, Construction of covalent organic frameworks via three-component one-pot Strecker and Povarov reactions, J. Am. Chem. Soc. 142 (14) (2020) 6521–6526.
[31] Q. An, H.-e Wang, G. Zhao, S. Wang, L. Xu, H. Wang, Y. Fu, H. Guo, Understanding dual-polar group functionalized COFs for accelerating li-ion transport and dendrite-free deposition in lithium metal anodes, ENERGY Environ. Mater. 6 (2) (2023) e12345.
[32] C. Niu, W. Luo, C. Dai, C. Yu, Y. Xu, High-voltage-tolerant covalent organic framework electrolyte with holistically oriented channels for solid-state lithium metal batteries with Nickel-Rich cathodes, Angew. Chem. Int. Ed. 60 (47) (2021) 24915–24923.
[33] M.N. Jackson, S. Oh, C.J. Kaminsky, S.B. Chu, G. Zhang, J.T. Miller, Y. Surendranath, Strong electronic coupling of molecular sites to graphitic electrodes via pyrazine conjugation, J. Am. Chem. Soc. 140 (3) (2018) 1004–1010.
[34] J. Wang, Y. Lee, K. Tee, S.N. Riduan, Y. Zhang, A nanoporous sulfur-bridged hexaazatrinaphthylene framework as an organic cathode for lithium ion batteries with well-balanced electrochemical performance, Chem. Commun. 54 (55) (2018) 7681–7684.
[35] C. Peng, G.-H. Ning, J. Su, G. Zhong, W. Tang, B. Tian, C. Su, D. Yu, L. Zu, J. Yang, M.-F. Ng, Y.-S. Hu, Y. Yang, M. Armand, K.P. Loh, Reversible multi-electron redox chemistry of π-conjugated N-containing heteroaromatic molecule-based organic cathodes, Nat. Energy 2 (7) (2017) 17074.
[36] H. Banda, D. Damien, K. Nagarajan, A. Raj, M. Hariharan, M.M. Shaijumon, Twisted perylene diimides with tunable redox properties for organic sodium-ion batteries, Adv. Energy Mater. 7 (20) (2017) 1701316.
[37] Z. Lin, Y. Wang, Y. Li, Y. Liu, S. Zhong, M. Xie, F. Yan, Z. Zhang, J. Peng, J. Li, A. Wang, X. Chen, M. Zhai, H. Zhang, J. Qiu, Regulating solvation structure in gel polymer electrolytes with covalent organic frameworks for lithium metal batteries, Energy Storage Mater. 53 (2022) 917–926.
[38] A.J. Bard, L.R. Faulkner, Fundamentals and applications, Electrochem. Methods 2 (482) (2001) 580–632.
[39] X. Li, K.P. Loh, Recent progress in covalent organic frameworks as solid-state ion conductors, ACS Mater. Lett. 1 (3) (2019) 327–335.
[40] A.M. Pütz, M.W. Terban, S. Bette, F. Haase, R.E. Dinnebier, B.V. Lotsch, Total scattering reveals the hidden stacking disorder in a 2D covalent organic framework, Chem. Sci. 11 (47) (2020) 12647–12654.
[41] M. Li, M. Kolek, J.E. Frerichs, W. Sun, X. Hou, M.R. Hansen, M. Winter, P. Bieker, Investigation of polymer/ceramic composite solid electrolyte system: the case of PEO/LGPS composite electrolytes, ACS Sustain. Chem. Eng. 9 (34) (2021) 11314–11322.
[42] Y.-W. Song, S.-J. Park, K. Heo, H. Lee, D. Hwang, M.-Y. Kim, J. Kim, J. Lim, Enhancing electrochemical performance in PEO/LLZTO composite solid electrolyte via PEG polymer integration for solid-state batteries, Energy Technol. 11 (9) (2023) 2300334.
[43] W. Zhang, J. Nie, F. Li, Z.L. Wang, C. Sun, A durable and safe solid-state lithium battery with a hybrid electrolyte membrane, Nano Energy 45 (2018) 413–419.
[44] Z. Wang, Y. Zhang, P. Zhang, D. Yan, J. Liu, Y. Chen, Q. Liu, P. Cheng, M. J. Zaworotko, Z. Zhang, Thermally rearranged covalent organic framework with flame-retardancy as a high safety Li-ion solid electrolyte, eScience 2 (3) (2022) 311–318.
[45] J. Zheng, H. Dang, X. Feng, P.-H. Chien, Y.-Y. Hu, Li-ion transport in a representative ceramic–polymer–plasticizer composite electrolyte: Li7La3Zr2O12–polyethylene oxide–tetraethylene glycol dimethyl ether, J. Mater. Chem. A 5 (35) (2017) 18457–18463.
[46] W. Tang, T. Zhao, K. Wang, T. Yu, R. Lv, L. Li, F. Wu, R. Chen, Dendrite-free lithium metal batteries enabled by coordination chemistry in polymer-ceramic modified separators, Adv. Funct. Mater. 34 (2024) 2314045.
[47] O. Sheng, J. Zheng, Z. Ju, C. Jin, Y. Wang, M. Chen, J. Nai, T. Liu, W. Zhang, Y. Liu, X. Tao, In situ construction of a LiF-enriched interface for stable all-solid-state batteries and its origin revealed by Cryo-TEM, Adv. Mater. 32 (34) (2020) 2000223.
[48] Y. Su, X. Zhang, C. Du, Y. Luo, J. Chen, J. Yan, D. Zhu, L. Geng, S. Liu, J. Zhao, Y. Li, Z. Rong, Q. Huang, L. Zhang, Y. Tang, J. Huang, An all-solid-state battery based on sulfide and PEO composite electrolyte, Small 18 (29) (2022) 2202069.